Molecular Dynamics Simulations of Hydrophilic Pores in Lipid Bilayers

Hari Leontiadou, Alan E. Mark, and Siewert J. Marrink
Department of Biophysical Chemistry, University of Groningen, Nijenborgh, Groningen, The Netherlands

ABSTRACT Hydrophilic pores are formed in peptide free lipid bilayers under mechanical stress. It has been proposed that the transport of ionic species across such membranes is largely determined by the existence of such meta-stable hydrophilic pores. To study the properties of these structures and understand the mechanism by which pore expansion leads to membrane rupture, a series of molecular dynamics simulations of a dipalmitoylphosphatidylcholine (DPPC) bilayer have been conducted. The system was simulated in two different states; first, as a bilayer containing a meta-stable pore and second, as an equilibrated bilayer without a pore. Surface tension in both cases was applied to study the formation and stability of hydrophilic pores inside the bilayers. It is observed that below a critical threshold tension of ~38 mN/m the pores are stabilized. The minimum radius at which a pore can be stabilized is 0.7 nm. Based on the critical threshold tension the line tension of the bilayer was estimated to be $\sim 3 \times 10^{-11}$ N, in good agreement with experimental measurements. The flux of water molecules through these stabilized pores was analyzed, and the structure and size of the pores characterized. When the lateral pressure exceeds the threshold tension, the pores become unstable and start to expand causing the rupture of the membrane. In the simulations the mechanical threshold tension necessary to cause rupture of the membrane on a nanosecond timescale is much higher in the case of the equilibrated bilayers, as compared with membranes containing preexisting pores.

INTRODUCTION

The physical and dynamical behavior of lipid bilayers is of fundamental importance in biological systems. The most basic property of lipid bilayers in biology, that of acting as a barrier between the inside and outside of a cell, depends strongly on the continuity of the bilayer structure. However, there are important biological processes such as the transport of small molecules across the membrane, fusion, budding events, and cell lysis that involve the partial breakdown of the lipid matrix. One important structure in which the continuity of the lipid matrix is lost (at least locally) is the formation of a water channel, or pore. It is well known that certain proteins and peptides are able to create channels and in this way selectively regulate the permeability and stability of membranes. It is less well known that ions and protons also permeate protein free lipid bilayers at rates in excess of that expected from simple diffusion. It has been suggested therefore that water pores can form transiently in protein free bilayers due to thermal and mechanical fluctuations (Jansen and Blume, 1995; Deamer and Bramhall, 1986; Lawaczeck, 1988). The presence of such pores could facilitate the passive transport of polar molecules across membranes as well as being initiation sites for structural defects associated with phase transitions, cell fusion, and lysis.

Electroporation and pipette aspiration experiments have been used extensively to study the formation and expansion of water pores in protein free lipid bilayers. Model membranes, vesicles and cells of different size and chemical composition have been used to study the phenomenon of membrane permeabilization under high electric fields and/or mechanical stress (Melikov et al., 2001; Tekle et al., 2001; Akinlaja and Sachs, 1998). The exact mechanism of pore formation due to electrocompressive stress is not completely understood. It is consistently found, however, that rupture of the membrane occurs at a critical transmembrane potential. Irreversible membrane breakdown (rupture) is believed to occur when the pore expands beyond a critical radius. In cases where the radius is below a critical value spontaneous resealing will occur. This is known as reversible electrical breakdown. The threshold for electroporation of a lipid bilayer depends strongly on the type of the model membrane and the duration and strength of the applied electrical pulse. Furthermore, experiments have shown that it is possible to control the evolution of these defect structures by applying surface tension to the membrane (Zhelev and Needham, 1993). The critical membrane tension for mechanical breakdown of electroporated SOPC liposomes was found to be ~1–2.8 mN/m. At this tension large pores with a radius of 2–12 μm were stable for several seconds. It was observed that all porated membranes break down at lower tensions than the respective nonporated membranes. Recently it has been shown that the process of pore formation and expansion is primarily a kinetic process (Evans and Heinrich, 2003). Thus the critical tension necessary for rupturing a membrane depends strongly on the loading rate of the applied tension. At high loading rates (25 mN/m per second) the critical tension for a DOPC membrane ranges between 10 and 20 mN/m, whereas at low loading rates (0.07 mN/m per second) it is 4 mN/m.

A number of theoretical models have been proposed to describe the formation and evolution of these meta-stable pores (Barnett and Weaver, 1991; Glaser et al., 1988; Freeman et al., 1994). All are based on the idea that mechanical or electrocompressive stress generates defects in the lipid area. The initial pores that form are believed to be small and

Submitted June 24, 2003, and accepted for publication October 13, 2003.

Address reprint requests to Siewert J. Marrink, E-mail: s.j.marrink@chem.rug.nl.

0006-3495/04/04/2156/09 $2.00

hydrophobic with the lipid tails exposed to water. The lipids then reorient, lining the water channel, to form a hydrophilic pore. In such simplified models the free energy of formation, E, of a cylindrical pore with a radius, r, is approximated by

$$E(r) = 2\pi r\gamma - \pi r^2\Gamma, \quad (1)$$

where γ is the line tension that opposes the creation of the pore and Γ is the surface tension that lowers the energetic barrier for pore creation and expansion. Therefore, changes in the surface tension of the membrane can either stabilize or destroy the meta-stable hydrophilic pores. From experimental data and theoretical studies it has been suggested that the critical radius for the formation of a hydrophilic pore is 0.3–0.5 nm. Simulation studies using simplified models have shown that it is possible to observe pore formation and closure (Groot and Rabone, 2001; Shillcock and Seifert, 1998). Shillcock and Seifert have used a two-dimensional fluid membrane model to study the formation of thermally induced pores. In their Monte Carlo simulations, lipids are represented by hard disks connected to each other, creating a fluid-like network. A more realistic model has been used recently by Groot and Rabone to study the effect of surfactants on the stability of lipid bilayers. Their model consists of beads that represent three carbon atoms or one water molecule. The dissipative particle dynamics method was used to relate the parameters of this simplified model to specific chemical details of the system. In general it is possible to obtain qualitative results by using coarse-grained and simplified models. However, the absence of the atomistic details of the system results in the loss of any quantitative information.

Hydrophilic pores have also been observed in simulations at atomic detail. During the spontaneous aggregation of lipids into bilayers, transient pores are observed as meta-stable intermediate structures (Marrink et al., 2001). Their lifetime ranged from 5 ns to 80 ns. In addition we recently reported atomistic simulations of DPPC bilayers in which pore formation was induced spontaneously on a nanosecond timescale (Tieleman et al., 2003). This was achieved either by applying a large mechanical tension or by the application of a strong electrical field. The pores induced by these methods led to irreversible breakdown of the membrane.

In this study we present extended, atomistic molecular dynamics (MD) simulations that have been conducted to enable us to understand, in detail, the structure and dynamics of transient membrane pores. The mechanism of pore stabilization and expansion under stress is investigated. Furthermore the passive transport of water molecules through the pores is calculated and the size and shape of these structures is characterized.

METHODS

Simulation of the membrane

A dipalmitoylphosphatidylcholine (DPPC) bilayer was chosen for this work because it is well studied experimentally and computationally. The force field used for DPPC was similar to that used by Lindahl and Edholm (2000). The GROMOS force field (van Gunsteren, et al., 1996; 1998) was used for the description of all bonds, angles, and improper dihedrals. The van der Waals interaction parameters of the united CHn atoms of the lipid tails were adjusted to pentadecane (Berger et al., 1997). For the electrostatic interactions the fractional charges suggested by Chiu et al. (1995) were used. The water was described by the simple point charge model (Berendsen et al., 1981). The MD simulations were performed using the GROMACS package version 3.05 (Lindahl et al., 2001). Periodic boundary conditions were applied and the temperature was coupled to 323 K. This is above the phase transition of DPPC, which is at 315 K. In all simulations the pressure in the direction normal to that of the membrane was kept constant at 1 bar (Berendsen, et al., 1984). To impose a surface tension onto the system the lateral pressure was varied systematically from −10 to −1000 bar. To evaluate the nonbonded interactions a group-based, twin-range cutoff scheme was used. Lennard-Jones and electrostatic interactions within a short-range cutoff of 1.0 nm were updated every step. Long-range electrostatic interactions within a cutoff of 1.5 nm were updated every 10 steps together with the pair list. For comparison, simulations were also performed including a reaction-field correction to account for the truncation of the long-range electrostatic interactions (Tironi et al., 1995). A 5-fs time step was used (Feenstra et al., 1999). Bond lengths were constrained using the LINCS algorithm (Hess et al., 1997). The system consisted of 128 DPPC lipids and 6029 water molecules.

An overview of the simulations performed is given in Table 1. The initial structure of the system was taken from a previous simulation of the

TABLE 1 Summary of the simulation parameters

Label	P_{Lat} (bar)	Surface tension (mN/m)	$\langle L_z \rangle$ (nm)	Time (ns)	A_{lipid} (nm^2)
Stxy0	0	0	8.6	50	
Stxy10	−10	9	8.4	50	
Stxy20	−20	17	8.2	50	
Stxy30	−30	25	8.0	158	
Stxy40	−40	32	7.8	110	
Stxy50	−50	38	7.5	125	
Stxy60*	−60	34	5.7	50	
Stxy70*	−70	35	5.1	37	
Stxy80*	−80	39	5.0	23	
Stxy90*	−90	38	4.3	23	
Stxy100*	−100	19	4.3	16	
Eqxy0	0	0	8.8	48	0.62
Eqxy10	−10	10	8.7	47	0.63
Eqxy20	−20	18	8.4	50	0.64
Eqxy30	−30	25	8.3	50	0.66
Eqxy40	−40	33	8.0	35	0.67
Eqxy50	−50	39	7.8	46	0.69
Eqxy100	−100	68	6.8	48	0.81
Eqxy150	−150	84	5.6	54	0.99
Eqxy200*	−200	90	4.6	15	1.2†
Caxy30	−35	27	7.9	100	
Caxy40	−43	32	7.7	50	
Caxy50	−55	39	7.4	100	
Caxy70	−55	35	6.3	45	

Simulations of the bilayer with the pore under tension are labeled as Stxy and the number of the lateral pressure applied to the system as Stxy0–100. The label Eqxy corresponds to simulations where the equilibrated bilayer without a pore is simulated under tension (Eqxy0–200). The label Caxy refers to constant area simulations (Caxy30–70). P_{Lat} is the average lateral pressure applied perpendicular to the membrane. L_z is the size of the simulation box in the direction normal to that of the membrane. A_{lipid} is the area per lipid for the bilayer without a pore.

*Rupture occurs.

†Area per lipid before pore formation and expansion.

spontaneous formation of a DPPC bilayer (Marrink et al., 2001). Two starting conformations were used in this study. One was an equilibrated bilayer and the other a bilayer that contained a hydrophilic pore formed during the process of aggregation. Both of the systems were simulated under a range of different surface tensions as well as under stress-free conditions (zero surface tension). A series of simulations was also performed at constant surface area. The starting structures for these simulations were taken from the simulations of the bilayer under tension.

Analysis

The surface tension, Γ, in the simulations was calculated from the external pressure applied to the system as $\Gamma = L_z (P_z - \langle P_{Lat} \rangle)$ where L_z is the length of the simulation box in the z-direction, P_z is the pressure along the z axis, and P_{Lat} the average of the lateral pressure (in the x,y plane).

The water pores studied in this work are very dynamic structures. To accurately determine their size and shape, all properties were averaged over long periods of simulation time (50–100 ns). To estimate the absolute size of the stabilized pores we calculated the difference in the average number of water molecules in the membrane between the bilayer with a pore and that without, under the same conditions. By integrating across the bilayer, the total number of water molecules N_{total} inside the pore could be estimated. The region between the peaks in the lipid density distribution was integrated over, which corresponds roughly to the positions of the phosphate groups at the interface (see Fig. 3). As the shape of the pores is nonuniform across the membrane, the number of water N_{water_I} (and lipid N_{lipids_I}) molecules only in the central region of the pore was also calculated. The central region was defined as ± 0.85 nm either side of the center of the bilayer. By averaging this property every nanosecond it is possible to estimate the fluctuations in the relative size of the central pore region. To estimate the area of a pore ($A_{cylinder}$) it is necessary to make some assumptions in regard to its shape and the density of water molecules inside the pore. The central part of a pore was assumed to be perfectly cylindrical in shape, containing N_{water_I} water molecules at the same density as bulk water. The stated pore area therefore reflects the area of the pore in the membrane interior. The regions used in this analysis are indicated in Fig. 1.

The number of water molecules that pass through the equilibrated pores was calculated by assuming that there were two boundaries at the edges of the pore (see Fig. 1). A water molecule was considered to have permeated the membrane if it crossed both of these two artificial boundaries. This yields the number of flux events in both directions. The average flux, over a period of 50 ns, was used to estimate the rate of permeation of the membrane. The permeability coefficient was calculated from the equation $P = J/\Delta C$, where J is the flux and ΔC the concentration gradient. The flux was estimated as described above and the concentration gradient was taken as equal to 55.5 mol/L.

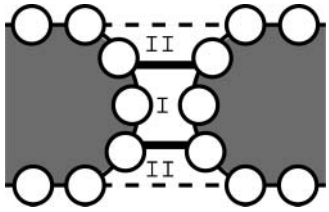

FIGURE 1 Cartoon of a water pore in the interior of the bilayer. Two regions are distinguished. Region I is the interior of the pore defined as the region ± 0.85 nm from the bilayer center. Region II is the pore opening or interfacial region. The boundary between region II and the bulk water is taken as the peak in the electron density profile of the membrane. This corresponds roughly to the position of the phosphate groups (see Fig. 3).

RESULTS

Structure of the stabilized pores

A side view of the pore created during the spontaneous formation of the DPPC bilayer is given in Fig. 2 *a*. The membrane is curved at the ends of the pore and the lipids are perturbed around it. In Fig. 2 *b* a slice of the interior of the membrane containing the pore without the water molecules is shown. Under stress-free conditions, this water bridge is stable in the membrane for up to 100 ns. Gradually the pore collapses and the bilayer becomes continuous.

However, when a surface tension is imposed onto the system the behavior of these channels changes significantly. In simulations of the membrane in which the lateral pressure was between -50 bar ($\sim$38 mN/m) and -10 bar ($\sim$10 mN/m) the pores appear to be stable (on the timescale of our simulations $\sim$160 ns) and their structural characteristics can be analyzed. In Fig. 3 the distribution of water and lipid molecules along the normal of the membrane is illustrated. Distributions are shown both for a bilayer containing a pore and for a bilayer without a pore simulated under the same tension. The difference between the water density profiles in these two systems (*shaded region*) reveals the distribution of water molecules inside the pore. This distribution is clearly not constant. A higher water density is found near both interfaces, at the pore openings. This is consistent with the pore having an hourglass shape.

The absolute number of water molecules N_{total} inside the pore was estimated by integrating the water density distribution inside the pore across the membrane. The boundaries of the membrane were taken as the peaks in the electron density profiles as shown in Fig. 3. The results are summarized in Table 2. Under stress-free conditions the water pore contains $\sim$92 water molecules. More water molecules enter the pore when the membrane is under tension. The size of the pore increases to 163–180 molecules for tensions between 9 and 32 mN/m. However, when the tension reaches a value of 38 mN/m the number of water molecules in the interior of the membrane increases to 224.

To analyze the size and shape of the pore in more detail, the number of water molecules N_{water_I} and lipid headgroups

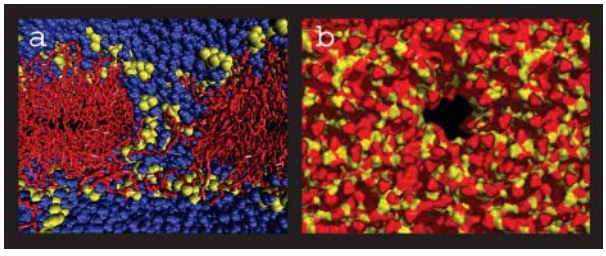

FIGURE 2 Side (*a*) and top (*b*) views of 128 DPPC lipids in a bilayer containing a preformed pore used as the starting structure for later simulations. The lipid headgroups are shown in orange, lipid tails in red, and water molecules in cyan. Water molecules are removed from the top view for clarity.

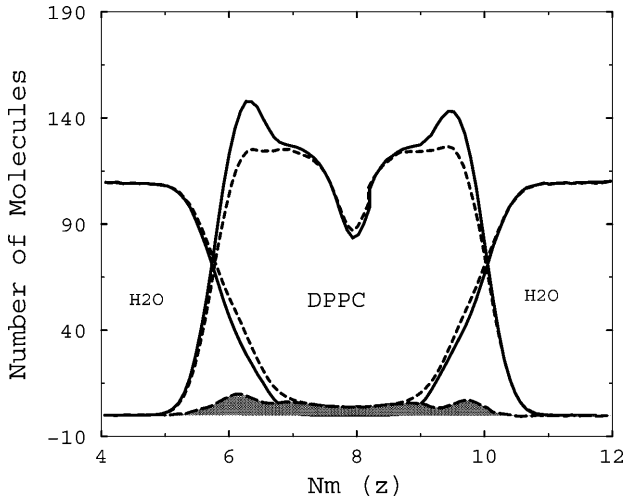

FIGURE 3 The average number of water molecules in the membrane. Dotted lines correspond to the distributions of the lipids and water molecules in the membrane with the pore. The solid lines correspond to the equilibrated bilayer without a pore. The difference between the two water distributions is indicated by the dashed lines. The integral of this line (*shaded area*) corresponds to the absolute size of the pore.

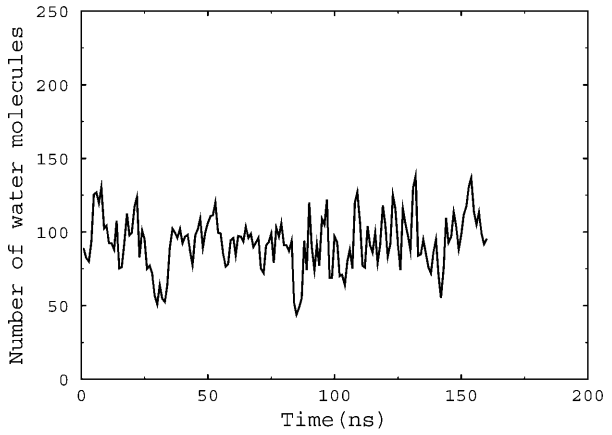

FIGURE 4 The number of water molecules in the central region of the pore as a function of time for the simulation with a lateral pressure of −30 bar (~25 mN/m).

$N_{\text{lipids\_I}}$ in the central region of the pore (see Fig. 1) was calculated. These results are also summarized in Table 2. At zero tension the interior of the pore contains ~85 water molecules and 7 lipid headgroups. The amount of interior water increases only slightly as the tension is increased (98 water molecules at 32 mN/m). The number of lipid headgroups does not change. However, when the tension reaches 38 mN/m both the number of water molecules (124) and lipid headgroups (9) increase significantly. The values presented in Table 2 are 50-ns averages as the pore is highly dynamic. Fig. 4 shows the dependence of the relative number of water molecules in the central region of the pore on time, for the simulation under a lateral pressure of −30 bar (~25 mN/m). Notice that although the size of the pore fluctuates rapidly around the mean value, the overall structure remains stable. This holds for all simulations with a surface tension below the critical value of 38 mN/m.

TABLE 2 Parameters indicating the size and shape of the pores

Label	Surface tension (mN/m)	N_{total}	$N_{\text{water\_I}}$	$N_{\text{lipids\_I}}$	H_2O/ns	A_{cylinder} (nm^2)	Flux (H_2O/ns per nm^2)
Stxy0	0	92	85 ± 13	7 ± 2	4 ± 1	1.5	3 ± 1
Stxy10	9	184	98 ± 15	7 ± 2	6 ± 1	1.7	3 ± 1
Stxy20	17	163	99 ± 15	8 ± 2	8 ± 3	1.8	4 ± 2
Stxy30	25	173	93 ± 19	7 ± 2	9 ± 2	1.7	5 ± 1
Stxy40	32	176	98 ± 17	7 ± 2	12 ± 2	1.9	6 ± 1
Stxy50	38	224	124 ± 27	9 ± 2	23 ± 6	2.5	9 ± 2
Caxy30	27		87 ± 19	7 ± 2	10 ± 3	1.7	6 ± 2
Caxy40	32		100 ± 18	7 ± 2	14 ± 1	1.9	7 ± 1
Caxy50	39		123 ± 19	8 ± 2	21 ± 2	2.5	8 ± 1
Caxy70	35		356 ± 30	12 ± 2	202 ± 10	8.5	24 ± 1

N_{total} is the total number of water molecules inside the pore in regions I and II. $N_{\text{water\_I}}$ and $N_{\text{lipids\_I}}$ correspond to the number of molecules in the central part of the pore in region I (see Fig. 1). Note that A_{cylinder} is an estimation of the area of the pore based on assumptions described in Methods.

The area of the pore was calculated as described in Methods. Under stress-free conditions the radius of the pore in the interior of the bilayer is ~0.7 nm. The radius increases slowly to ~0.9 nm at the critical surface tension. For the porated bilayers stabilized under lateral pressures of −30, −40, and −50 bar, constant area simulations have also been conducted. Starting from the preformed pores that were equilibrated under constant surface tension the area was fixed and the system allowed to evolve. The details of the simulations are given in Table 1. Note that after equilibration the lateral pressure is almost the same in all systems. The relative number of water molecules in the middle of the membrane was estimated and the averaged values are presented in Table 2. In all cases the pore remains more or less constant during the 50–100-ns simulation. The pores show no tendency to close. A constant area simulation was also performed for the bilayer under a pressure of −70 bar. The starting configuration for this simulation was a frame taken 4 ns after tension had been applied to the bilayer, at a time when the pore was already enlarged. The pore was allowed to equilibrate for 45 ns at this area. Note that the average lateral pressure drops from −70 bar to −55 bar, although the relative size of the pore does not change significantly.

The flux of water molecules that pass through the equilibrated pores is also given in Table 2. For the simulations under constant surface tension it is observed that there is a small systematic increase in the flux as the tension rises. The flux increases markedly when the tension is high (38 mN/m). The simulations at constant area give similar results. The flux is slightly enhanced, however, for the case of Caxy30 and Caxy40 as compared to Stxy30 and Stxy40, respectively. Note that the flux is greatly increased when the

pore is large and expanded as in the case of Caxy70. The permeability coefficient of a single pore was calculated to be in the range of 7×10^{-13} cm^3/s for the Stxy50 simulation and 2×10^{-13} cm^3/s for the simulation Stxy10.

Membrane rupture

When the applied pressure is more than a critical value of –50 bar (~38 mN/m), the bilayer that contains a preformed pore becomes highly unstable. The time evolution of the relative size of the pore under different tensions is illustrated in Fig. 5. When the lateral pressure is high enough the pore expands. More water molecules penetrate the membrane whereas the bilayer thickness does not change significantly. The process continues until the lipid bilayer is completely disrupted. The mechanism by which pore expansion leads to the rupture of the membrane is similar for all the simulations Stxy60–100. Nevertheless, the time lag before the pore starts to grow, becomes less as the lateral pressure is increased. In the Stxy60 simulation the pore starts expanding after 15 ns whereas for Stxy100 only 4 ns are needed. The process of pore expansion is illustrated in Fig. 6 for a membrane under a lateral pressure of −60 bar (~34 mN/m). Initially the minimum distance between the lipid headgroups that are in the middle of the pore is ~0.3–0.5 nm and it can be seen that the lipids within the pore are quite disordered. The size of the pore remains stable for the first 15 ns, and then starts to grow. More water molecules concentrate in the membrane whereas the lipid headgroups move in and line the pore. The radius of the pore continues to increase until the rupture of the membrane after ~30 ns. Notice that the thickness of the bilayer remains the same. Although the lipid headgroups within the pore rearrange during the expansion, their relative population is constant.

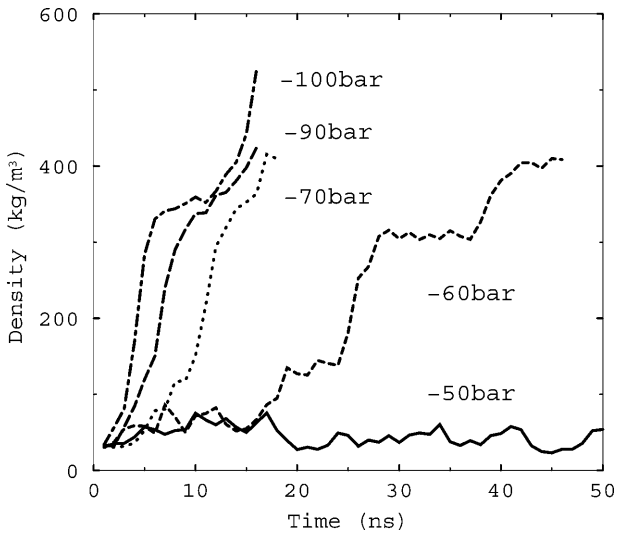

FIGURE 5 Average relative water densities in the middle part of the pore for different lateral pressures. The solid line is for the simulation with lateral pressure of −50 bar, the dashed line is for −60 bar, the dotted line for −70 bar, the long dashed for −90 bar, and the dotted-dashed line for the simulation under pressure of −100 bar. Note that above a certain threshold tension (38 mN/m), pores start to expand. Within few nanoseconds (4–20 ns) the small bilayer is destroyed.

Starting from an equilibrated DPPC bilayer without any pore, we also investigated the stability of the membrane as a function of the applied pressure. Although the area per lipid (see Table 1) deviates from its equilibrium value (~0.6 nm^2) as the lateral pressure increases, rupture does not occur even at pressures as high as –150 bar. The area expansion of the bilayer under low tension (9 mN/m) is ~1–3%, in agreement with experimental measurements (Needham et al., 1988). Only when the pressure reaches the value of −200 bar, do the lipids start to rearrange significantly. The fluctuations induced in the lipid matrix result in the formation of a water channel in the membrane. In Fig. 7 the formation and expansion of this channel is illustrated. The starting conformation is the equilibrated DPPC bilayer. During the first few nanoseconds the membrane thins and the area almost doubles (~1.2 nm^2). After ~12 ns a pore is formed. The distance between the lipid headgroups in the middle of the pore is initially ~0.5 nm but it grows rapidly. Within 2 ns after the formation of the pore, the membrane is severely disrupted. Pore formation starts with the penetration of water molecules from both sides of the membrane. When the water molecules meet in the middle of the bilayer a complete water channel is created. Once the pore has formed, the mechanism of further expansion and membrane rupture is the same as that described previously.

DISCUSSION

As expected from the existing theoretical models which predict the existence of a minimum in the free energy of the pore as a function of pore radius, we find that pores formed as intermediates during the spontaneous aggregation of a DPPC lipid bilayer can be stabilized by the application of mechanical tension. The minimum radius of such pores is ~0.7 nm. Above a critical tension (~38 mN/m) the pores become unstable and membrane rupture occurs. The same type of pores can be formed starting from an equilibrated bilayer if the tension is sufficiently high. Because the time required for pore formation at tensions close to the critical one is very slow compared with the simulation timescale, a high tension (~90 mN/m) must be applied to accelerate the process. In this way spontaneous pore formation can be observed. However, this results in significant thinning of the bilayer before pore formation. The pore itself is very unstable and rupture occurs within only 2 ns. In our simulations the critical tension at which rupture occurs is higher than the reported experimental values. In general lipid bilayers are known to rupture under tensions that are ~1–25 mN/m. However, rupture is a dynamical process and depends strongly on the rate at which loading is applied (Evans and Heinrich, 2003). Increasing the loading rate

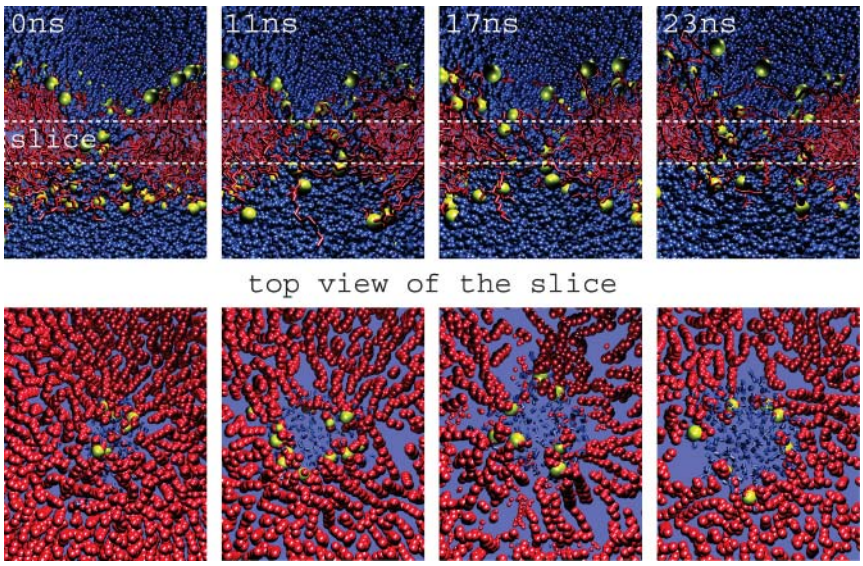

FIGURE 6 Snapshots of the process of pore expansion, for a given lateral pressure (−60 bar). The orange spheres represent the phosphate group of the lipid headgroups whereas the lipid tails are colored in red. The water molecules are shown in blue. The starting structure was a DPPC bilayer containing a preformed pore. Pictures show the side and top views of a slice of the interior of the membrane. Initially, the pore is quite small. In time the pore expands and after ~30 ns the pore occupies most of the simulation box. The membrane is considered to have ruptured.

shifts the tension at which rupture occurs to higher values. For DOPC and SOPC vesicles it is found that the rupture tension increases by a factor of 4 when the loading rate is increased by 3 orders of magnitude. Using a kinetic model, Evans and Heinrich have shown that two regimes can be distinguished for membrane rupture. At low loading rates, the kinetics of rupture are determined by the rate at which the pore can expand, whereas at high loading rates the formation of the pore itself becomes rate-limiting. Thus, at high loading rates the tension required for pore formation is relatively high and inevitably leads to membrane rupture. This is what is observed in our simulations of pore formation in equilibrated bilayers, where the effective loading rate is very high. The timescale at which pores form and membranes rupture in biological systems under low tensions is still beyond that achievable using fully atomistic molecular dynamic simulation techniques. At low loading rates, the kinetic model predicts that the height of the barrier to pore expansion is tension-dependent. At a critical threshold tension the kinetic impedance disappears. Fitting their experimental measurements on DOPC and SOPC vesicles to the kinetic theory, Evans and Heinrich (2003) estimate this critical tension to be between 30 and 100 mN/m. The value of 38 mN/m that we find for unimpeded pore expansion of a DPPC membrane is within this range.

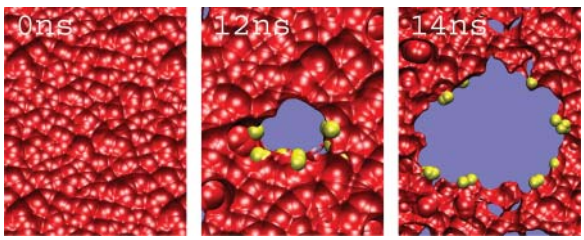

FIGURE 7 Formation and expansion of a water pore in an equilibrated DPPC bilayer under lateral pressure of −200 bar (~89 mN/m). The slices represent the middle part of the pore and have a thickness of ~0.8 nm. The phosphate groups of the lipid tails are shown in orange spheres and the tails in red. Water molecules are removed for clarity. The pores once formed are very unstable. They rapidly start to expand and eventually destroy the membrane.

From the critical tension we can estimate the line tension of the membrane. At the critical tension Γ^* the free energy change upon pore expansion dE/dr is zero. Using the simple free energy expression given in Eq. 1 the line tension γ is then given by

$$\gamma = r^* \times \Gamma^*, \tag{2}$$

where r^* denotes the radius of the pore at the onset of expansion. At the critical tension of $\Gamma^* = 38$ mN/m the radius of the pore was estimated to be $r^* = 0.9$ nm, resulting in a line tension for our DPPC membrane of $\gamma \sim 3 \times 10^{-11}$ N. This value agrees well with the value of 1×10^{-11} N reported by Zhelev and Needham (1993), based on experimental measurements. It is interesting to point out that the line tension appears to be smaller closer to the opening of the pore. Table 2 shows that, for tensions lower than the critical tension, the opening of the pore expands whereas the pore interior remains essentially unchanged. This effect is probably a consequence of the curvature along the pore not being constant. Although the curvature perpendicular to the membrane does not change, the lateral curvature of the pore is much larger in the middle of membrane than at the rim. Therefore, the line tension at both pore openings is less, allowing it to expand at lower tensions.

To test the dependence of the results on the force field used in the simulations, additional simulations were performed in which a reaction-field correction (Tironi et al., 1995) was included in the calculation of the long-range electrostatic interactions (see Methods). Including a reaction-field correction avoids the artificial correlations that are seen

when using the cutoff methods (C. Anezo et al., 2003). Qualitatively the results found are the same. However, with the reaction-field correction the pores appear less stable. The critical tension at which expansion occurs falls to ~18 mN/m, a difference of 20 mN/m compared to the straight cutoff simulations. At lower tensions the pores remain stable with the same properties as was observed when using just a cutoff. The effect of the reaction-field correction therefore is a reduction of the line tension by roughly a factor of 2 (bringing it closer to the experimental values). The different properties of the reaction-field bilayer are also reflected in the area per headgroup. For an equilibrated bilayer the area increases from 0.62 to 0.66 nm^2 upon including a reaction-field correction. Interestingly, when simulating with a straight cutoff a similar area of 0.66 nm^2 is obtained at tensions of ~20 mN/m (see Table 2). Compared to the simulations using a straight cutoff, the simulations including a reaction-field correction can be seen as equivalent to a bilayer under an effective tension of 20 mN/m, with respect to the conditions under which the model was originally parameterized.

In Fig. 8 a cartoon is presented summarizing the effect of tension on the structure and stability of the pore as observed in the simulations. At zero tension, a bilayer without a pore is the most thermodynamically stable state (Stxy0). At small tensions, pores can be stabilized inside the bilayer (Stxy10–40). When the tension is increased, the pore expands slightly. This expansion takes place predominantly at the pore openings. Once the critical tension is reached (Stxy50), expansion of the pore occurs at no free energy cost, and pores of any size can be trapped (Caxy70). Above the critical tension, the pores are unstable and will grow unhindered, leading to the rupture of the membrane (Stxy60–100). A gradual thinning of the bilayer is concomitant with an increased tension.

It is interesting to compare the permeability of the stabilized hydrophilic pores with that of channels formed by proteins or small peptides. We observe ~6–24 water molecules per nanosecond passing through the pores that are stabilized at tensions below the critical tension. As expected, the magnitude of the flux correlates with the area of the pore and a larger flux is obtained for pores that are expanded, as in the simulation Caxy70. The flux through the nonexpanded pores corresponds to a single-channel permeability coefficient of $\sim 2\text{–}7 \times 10^{-13}$ cm^3/s. This is relatively close to the value of 1.1×10^{-12} cm^3/s reported for desformylgramicidin channel, a channel with an extremely high water permeation rate (Sarapov et al., 2000). The water permeability coefficient for a pure DPPC lipid vesicle is in the order of 10^{-4} cm/s. If the dominant mechanism for water permeation was via water pores, $\sim 10^8$ pores/cm^2 or 1 pore/10^6 lipids would be sufficient to account for the flux of water molecules through the vesicle. Assuming a surface density for water of the order of 10^{-9} mol/cm^2, this corresponds to a free energy of the pore of 40 kJ/mol. The generally accepted mechanism by which small neutral molecules permeate the membrane is diffusion through the membrane and not through water pores (Weaver et al., 1984). Forty kJ/mol thus represents a lower bound for the free energy of the pore. Typical permeation rates for ions are $\sim 10^{-12}$ cm/s. If it is assumed that the diffusion rate of ions through the pore is of the same order as that of water molecules, only 1 pore/cm^2 would be required to account for the permeation rate of ions. The corresponding free energy of the pore in that case is 90 kJ/mol. The assumption that the diffusion rate of ions

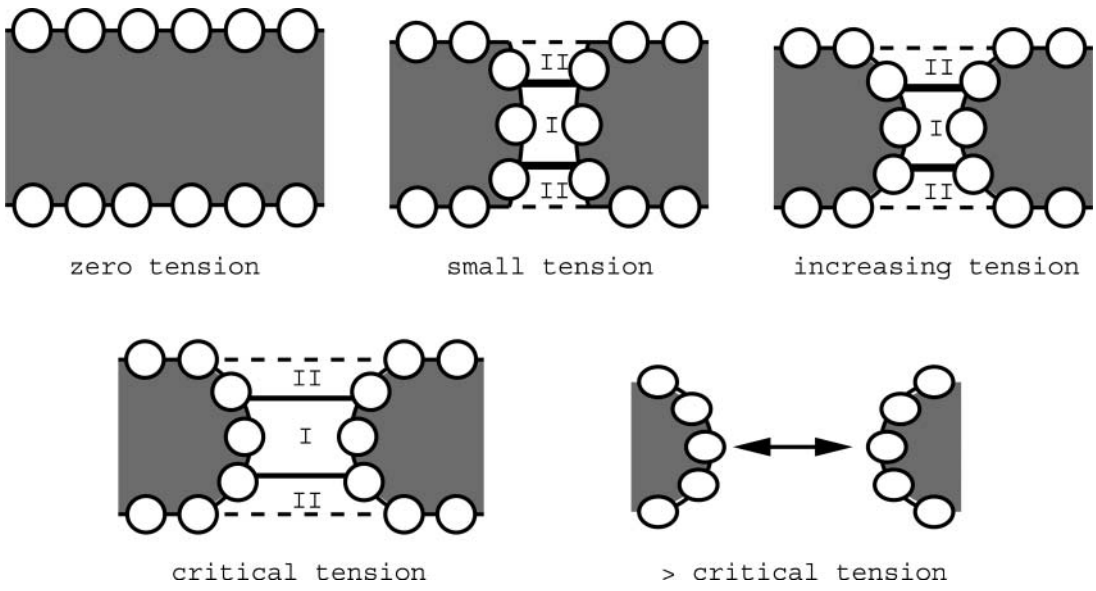

FIGURE 8 Cartoon summarizing the effect of tension on the stability and structure of the pore. We observe that at low tension the pores are stabilized. Increasing tension leads to the expansion of the pore that is more profound at the openings of the channel. When the tension is beyond a critical value, the pore becomes unstable and leads to the rupture of the bilayer.

through the pore is of the same order as the water might be an overestimation.

The above discussion of pore formation relates to pure lipid vesicles. The question that remains is whether spontaneous pore formation is significant in a biological context. In prebiotic systems it is probable that spontaneously formed pores played a role in the transport of ions and organic compounds. Modern cells, however, have evolved a variety of mechanisms to allow for and stabilize transient pores. For example, in hyposmotic conditions which lead to the swelling of cells and high membrane tension, the rupture of the cell is prevented by specialized mechanoselective proteins such as the MscL channels which open and prevent cell lysis. These proteins have evolved to gate just below the tension required for spontaneous pore formation (Moe et al., 2000; Colombo et al., 2003). A number of experimental studies indicate that peptides are capable of permeabilizing membranes by means of pore creation. The antimicrobial peptide magainin 2, for instance, imposes positive curvature strain to the membrane, resulting in the creation of a dynamic peptide-lipid complex pore (Matsuzaki, 1998). Membrane composition is also important for the stability of the pores in cell membranes. The presence of cholesterol or short-chain lipids influences the mechanical and thermodynamic properties of the membranes, altering in this way their barrier properties.

CONCLUSION

With atomistic MD simulations we were able to show that hydrophilic water pores can be stabilized in a DPPC lipid membrane under low tension. The pores are shaped like an hourglass, with a radius of $\sim$0.7 nm in the interior of the membrane. Lipid headgroups line the pore, which typically contains $\sim$100 water molecules. The water permeability coefficient of these pores is in the order of 10^{-13} cm^3/s per pore, similar to that of a gramicidin dimer channel. In accordance with experimental measurements and theoretical predictions, the pores become unstable when the tension is increased beyond a certain threshold. For the DPPC membrane simulated we find a critical tension of 38 mN/m. At this tension the line tension opposing pore expansion is overcome. The line tension is found to be $\sim 3 \times 10^{-11}$ N. At higher tensions the pore expands, leading to the rupture of the membrane. Pores can also be created in the bilayer by applying an even larger stress ($\sim$90 mN/m), in which case the creation of the pore is immediately followed by rupture.

REFERENCES

Anezo, C., A. H. de Vries, H. Holtje, D. P. Tieleman, and S. J. Marrink. 2003. Methodological issues in lipid bilayer simulations. *JPC-B*. 107:9424–9433.

Akinlaja, J., and F. Sachs. 1998. The breakdown of cell membranes by electrical and mechanical stress. *Biophys. J.* 75:247–254.

Barnett, A., and J. C. Weaver. 1991. Electroporation: a unified, quantitative theory of reversible electrical breakdown and rupture. *Bioelectrochem. Bioenerg.* 25:163–182.

Berendsen, H. J. C., J. P. M. Postma, W. F. van Gunsteren, A. Di Nola, and J. R. Haak. 1984. Molecular dynamics with coupling to an external bath. *J. Chem. Phys.* 81:3684–3690.

Berendsen, H. J. C., J. P. M. Postma, W. F. van Gunsteren, and J. Hermans. 1981. Interaction models for water in relation to protein hydration. *In* Intermolecular Forces. B. Pullman, editor. Reidel, Dordrecht, The Netherlands.

Berger, O., O. Edholm, and F. Jahnig. 1997. Molecular dynamics simulations of a fluid bilayer of dipalmitoylphosphatidylcholine at full hydration, constant pressure and constant temperature. *Biophys. J.* 72: 2002–2013.

Chiu, S., M. Clark, V. Balaji, S. Subramaniam, H. Scott, and E. Jakobsson. 1995. Incorporation of surface tension into molecular dynamics simulation of an interface: a fluid phase lipid bilayer membrane. *Biophys. J.* 69:1230–1245.

Colombo, G., S. J. Marrink, and A. E. Mark. 2003. Simulation of MscL gating in a bilayer under stress. *Biophys. J.* 84:2331–2337.

Deamer, D. W., and J. Bramhall. 1986. Permeability of lipid bilayers to water and ionic solutes. *Chem. Phys. Lipids.* 40:167–188.

Evans, E., and V. Heinrich. 2003. Dynamic strength of fluid membranes. *C. R. Physique.* 4:265–274.

Feenstra, A. K., B. Hess, and H. J. C. Berendsen. 1999. Improving efficiency of large time-scale molecular dynamics simulations of hydrogen-rich systems. *J. Comput. Chem.* 20:786–798.

Freeman, S. A., M. A. Wang, and J. C. Weaver. 1994. Theory of electroporation of planar bilayer membranes: predictions of the aqueous area, change in capacitance and pore-pore separation. *Biophys. J.* 67:42–56.

Glaser, R. W., S. L. Leikin, L. V. Chernomordik, V. F. Pastushenko, and A. L. Sokirko. 1988. Reversible electrical breakdown of lipid bilayers: formation and evolution of pores. *Biochim. Biophys. Acta.* 940:275–287.

Groot, R. D., and K. L. Rabone. 2001. Mesoscopic simulation of cell membrane damage, morphology change and rupture by nonionic surfactants. *Biophys. J.* 81:725–736.

Hess, B., H. Bekker, H. J. C. Berendsen, and J. G. M. Fraaije. 1997. LINCS: a linear constraint solver for molecular simulations. *J. Comput. Chem.* 18:1463–1472.

Jansen, M., and A. Blume. 1995. A comparative study of diffusive and osmotic water permeation across bilayers composed of phospholipids with different headgroups and fatty acyl chains. *Biophys. J.* 68:997–1008.

Lawaczeck, R. 1988. Defect structures in membranes: routes for the permeation of small molecules. *Ber. Bunsenges. Phys. Chem.* 92:961–963.

Lindahl, E., and O. Edholm. 2000. Mesoscopic undulations and thickness fluctuations in lipid bilayers from molecular dynamics simulations. *Biophys. J.* 79:426–433.

Lindahl, E., B. Hess, and D. van der Spoel. 2001. GROMACS 3.0: a package for molecular simulation and trajectory analysis. *J. Mol. Model.* 7:306–317.

Marrink, S. J., E. Lindahl, O. Edholm, and A. E. Mark. 2001. Simulation of the spontaneous aggregation of phospholipids into bilayers. *J. Am. Chem. Soc.* 123:8638–8639.

Matsuzaki, K. 1998. Magainins as a paradigm for the mode of action of pore-forming polypeptides. *Biochim. Biophys. Acta.* 1376:391–400.

Melikov, K. C., V. A. Frolov, A. Shcherbakov, A. V. Samsonov, Y. A. Chizmadzhev, and V. Chernomordik. 2001. Voltage-induced nonconductive pre-pores and meta-stable single pores in unmodified planar lipid bilayers. *Biophys. J.* 80:1829–1836.

Moe, P. C., G. Levin, and P. Blount. 2000. Correlating a protein structure with function of a bacterial mechanosensitive channel. *J. Biol. Chem.* 40:31121–31127.

Needham, D., T. J. McIntosh, and E. Evans. 1988. Thermomechanical and transition properties of dimyristoylphosphatidylcholine/cholesterol bilayers. *Biochemistry.* 27:4668–4673.

Saparov, M., Y. N. Antonenko, R. E. Koeppe, and P. Pohl. 2000. Desformylgramicidin: a model channel with an extremely high water permeability. *Biophys. J.* 79:2526–2534.

Shillcock, J. C., and U. Seifert. 1998. Thermally induced proliferation of pores in a model fluid membrane. *Biophys. J.* 74:1754–1766.

Tekle, E., R. D. Astumian, W. A. Friauf, and P. B. Chock. 2001. Asymmetric pore distribution and loss of membrane lipid in electroporated DOPC vesicles. *Biophys. J.* 81:960–968.

Tieleman, P. D., H. Leontiadou, A. E. Mark, and S. J. Marrink. 2003. Simulation of pore formation in lipid bilayers by mechanical stress and electric fields. *J. Am. Chem. Soc.* 125:6382–6383.

Tironi, I. G., R. Sperb, P. E. Smith, and W. F. van Gunsteren. 1995. A generalized reaction field method for molecular dynamics simulations. *J. Chem. Phys.* 102:5451–5459.

van Gunsteren, W. F., S. R. Billeter, A. A. Eising, P. H. Hunenberger, P. Kruger, A. E. Mark, W. R. P. Scott, and I. G. Tironi. 1996. Biomolecular Simulation: The GROMOS96 Manual and User Guide. vdf Hochschulverlag, ETH, Zurich, Switzerland.

van Gunsteren, W. F., X. Daura, and A. E. Mark. 1998. GROMOS force field. *In* Encyclopedia of Computational Chemistry, Vol. 2. P. von Rague Schleyer, editor. Wiley and Sons, Chichester, UK. 1211–1216.

Weaver, J. C., K. T. Powell, R. A. Mintzer, S. R. Sloan, and H. Ling. 1984. The diffusive permeability of bilayer membranes: the contribution of transient pores. *Bioelectrochem. Bioenerg.* 12:405–412.

Zhelev, D. V., and D. Needham. 1993. Tension-stabilized pores in giant vesicles: determination of pore size and pore line tension. *Biochim. Biophys. Acta.* 1147:89–104.